# A Paul Trap Mass Analyzer Consisting of Two Microfabricated Electrode Plates

Brett J. Hansen, [†] Zhiping Zhang, [‡] Ying Peng, [‡] Ivan W. Miller, [‡] Miao Wang, [‡] Milton L. Lee, [‡] Aaron R. Hawkins, [†] Daniel E. Austin[‡]

[†]*Department of Electrical and Computer Engineering, Brigham Young University, Provo, Utah, 84602*
[‡]*Department of Chemistry and Biochemistry, Brigham Young University, Provo, Utah, 84602*

## ABSTRACT

We report the design and performance of a novel radiofrequency (RF) ion trap mass analyzer, the planar Paul trap, in which a quadrupolar potential distribution is made between two electrode plates. Each plate consists of a series of concentric, lithographically deposited 100-micrometer-wide metal rings, overlaid with a thin resistive layer. To each ring is applied a different RF amplitude, such that the trapping field produced is similar to that of the conventional Paul trap. The accuracy and shape of the electric fields in this trap are not limited by electrode geometry nor machining precision, as is the case in traps made with metal electrodes. The use of two microfabricated plates for ion trap construction presents a lower-cost alternative to conventional ion traps, with additional advantages in electrode alignment, electric field optimization, and ion trap miniaturization. Experiments demonstrate the effects of ion ejection mode and scan rate on mass resolution for several small organic compounds. The current instrument has a mass range up to ~180 Thompsons (Th), with better than unit mass resolution over the whole range.

## INTRODUCTION

Since the invention of the radiofrequency (RF) quadrupole ion trap by Wolfgang Paul et al. in 1953,[1] quadrupole ion trap mass analyzers have played an increasingly important role in chemical and biological analyses. In addition to high sensitivity and specificity, ion traps combine reasonable simplicity of operation with complex functions such as multi-stage tandem mass analysis using a single analyzer. However, the hyperboloidal electrode shape of the original Paul trap is difficult to machine, especially on the miniaturized scale. As a result, significant effort has been spent on the development of alternative ion trap structures.

In 1998, Wells et al.[2] demonstrated a mass-selective instability scan on an ion trap with cylindrical geometry. The cylindrical ion trap, which had been introduced previously,[3, 4] simplified the hyperbolic ring electrode and end-cap electrodes with a cylindrical electrode and planar end-caps. This simplified trap geometry has facilitated and been the basis for most miniaturized ion trap systems.[5-10]

The performance of any ion trap depends to a large extent on the quality of the trapping electric field.[12] In

conventional mass analyzers, the electric field is determined by the shape and arrangement of a set of metal electrodes. Although curved (hyperboloidal) surfaces produce the most accurate electric fields, they are more difficult to fabricate accurately for miniaturized ion traps. Planar metal electrodes can be machined more easily, but even multiple planar electrodes, such as those used in rectilinear traps, must be accurately positioned and mounted. High performance in miniaturized ion traps requires accurate electric fields produced by geometrically simple electrode structures.

Recently, a novel ion trap mass analyzer was presented by Austin el al.,[13] which was based on a toroidal (circular) trapping geometry and microfabrication technology. The device, called the Halo ion trap, consisted of a pair of planar ceramic plates mounted in parallel, in which the facing surfaces were lithographically imprinted with sets of concentric ring electrodes, then covered with a layer of resistive germanium. The electric fields, established by applying different RF potentials to each ring, produced the same field shape as that in the toroidal ion trap. Although this type of mass analyzer is of promise due to its high ion storage capacity, sensitivity, and ease of fabrication and miniaturization, its performance (e.g., resolution and mass range) as presented was not optimal.

In the present work, the electrode approach of the Halo ion trap has been used to produce a mass analyzer of the Paul trap geometry. Whereas the electric fields of the Halo ion trap mimicked those of the toroidal trap, including a toroidal trapping volume, the electric fields in the present trap follow the design of the conventional Paul trap. Instead of the toroidal trapping volume of the Halo trap, ions in the present trap—the planar Paul trap—are confined to a small spherical volume at the device center. Although the larger trapping volume of the toroidal geometry is lost, the equations of ion motion are better understood in the Paul geometry. In particular, ion ejection is more straightforward.

Construction of an ion trap mass analyzer using two microfabricated plates provides several important advantages. For instance, two pieces can be mechanically aligned more easily than a larger number of electrode pieces. Polished flat plates have a smoother surface than traps made using other methods. Hence surface roughness, which has been identified as an issue for miniaturized traps,[14] is less of a problem. Microfabricated plates can be produced in quantity less expensively and more accurately than machined electrodes. The space between the plates provides convenient access for ionization sources, optics, pressure measurement, or other peripheral components. Finally, the use of an array of microfabricated electrode rings underneath a resistive layer allows the electric fields within the trap to be modified in a way that is not possible using machined electrodes.[15] Although the microfabricated plates themselves are fairly complex in both design and fabrication, other advantages make this approach potentially valuable.

## EXPERIMENTAL SECTION

### Plate Fabrication

Figure 1 shows the planar Paul ion trap implemented in this study. Each of the two trapping plates started as an aluminum oxide ceramic plate (99.6 % purity, Hybrid-Tek, Clarksburg, NJ) with dimensions of 46.95 × 36.20 × 0.635

mm. In each plate a central hole, laser-cut to 1 mm diameter, was used for ion ejection. Holes for electrical connections between the front and back sides of the plate (vias) were laser drilled to 127 μm diameter, arranged in a spiral pattern, each at an increasing distance from the central hole. Due to constraints in via hole drilling near an edge in the ceramic plates, the width of the first ring was 1.30 mm. From the second ring to the 24th ring, the width was 0.10 mm, as indicated in Table 1. Additional holes were cut to fit positioning rods and screws used for trap assembly and alignment. After laser cutting, the via holes were filled with a gold-tungsten alloy, and both sides of the alumina substrates were polished to a surface roughness of better than 1 μm. The active trapping area of each plate was evaporatively coated with a 100-nm layer of germanium, which prevented unwanted charge build-up and established a continuous, well-defined electric potential surface over the network of underlying rings. After deposition of germanium, the electrical resistance between adjacent rings was on the order of 10-100 MΩ. The other fabrication procedures were the same as that of the Halo ion trap, and a detailed description was given in a recent publication.[25]

**Experimental Setup**

Figure 1(b) shows the instrument setup for the experiments, including the electron gun assembly, trapping region, and the detector assembly. Behind each of the two ceramic plates comprising the trapping region was a printed circuit board (PCB) with a capacitor network. The capacitor network was used to establish the voltages on each of the ring electrodes under RF excitation. Spring-loaded pins were soldered to the PCB boards in order to make electrical contact with the back sides of the trapping plates. A 6-mm stainless steel spacer was mounted between the trapping plates. Holes in the spacer admitted the electron beam, sample vapor, helium gas, and a Teflon tube leading to a pirani gauge (Kurt J. Lesker, Clairton, CA). An RF signal with a frequency of 1.26 MHz and variable amplitude up to 738 $V_{0\text{-}p}$ (PSRF-100, Ardara Technologies, North Huntingdon, PA) was applied to the capacitor network on the PCBs, and the spacer was grounded during ion ejection. In addition, a supplementary low-voltage ac signal, generated using two 30 MHz synthesized function generators (DS345, Stanford Research Systems, Sunnyvale, CA) with $180^o$ phase difference, and amplified to 3.5 $V_{0\text{-}p}$ by a custom-made amplifier, was applied between the trapping plates to provide a dipole field for resonant ion ejection during the RF scan. The amplified supplementary ac signals were applied to the innermost ring on each plate, using a simple filter circuit to isolate the supplementary ac from the main RF signals. The applied frequency of the ac signal was 290 kHz, and $\beta_z$ was approximately 0.46. Other values of $\beta_z$ up to ~1 were also tested, with comparable mass resolution but reduced peak intensity.

Operational details of the planar Paul ion trap are given in Figure 2, which shows the time intervals and sequence for ionization, RF trapping, and ejection. First, the RF voltage was turned off to clear previously-trapped ions out of the trap. Then the RF was turned back on along with the electron gun, allowing sample to be ionized in the trapping volume. The electron gun was then turned off, allowing the ionized and trapped sample to collisionally cool. The

ejection ac was then turned on, and a voltage sweep of the drive RF was initiated. As the RF amplitude reached a level at which the secular frequency of any ion matched the applied supplementary ac frequency, that ion was resonantly ejected from the trap. Because ejection voltage was ramped from lower to higher voltages, ions were ejected in order of increasing *m/z* out of the trap. Once an ion was ejected through the hole in the trapping plates, it continued toward the detector. Ejected ions were detected using an ETP electron multiplier detector (SGE Analytical Science, Austin, TX), with a conversion dynode operated at -4000 V. The signal was amplified (427 Current Amplifer, Keithley Instruments, Cleveland, OH) and recorded using a digital oscilloscope (WaveRunner 6000A, LeCroy, Chestnut Ridge, NY).

In the experiments reported herein, helium was used as the buffer gas at an indicated pressure of $5.34 \times 10^{-3}$ Torr (uncorrected, 1 Torr = 133 Pa) as read from a pirani gauge (Kurt J. Lesker, Clairton, CA). Headspace vapor of the organic compounds of interest, without further purification, was leaked into the vacuum through two Swagelok leak valves (Swagelok, Solon, OH) to maintain a nominal pressure of $1.0\text{-}8.0 \times 10^{-5}$ Torr. In situ electron ionization was achieved using a custom-built electron gun comprising an iridium-tungsten filament, lens, gate, and a 1.6-amp power supply.

**Optimization of the electric field.** As shown in Figure 3(a), the planar Paul ion trap consists of two parallel ceramic plates with facing surfaces imprinted with concentric metal rings, overlaid with germanium. The metal rings superimpose a potential function on the germanium layer, which in turn establishes the three-dimensional potential distribution of the trapping region. This method of producing the trapping field is distinctive from the method used in conventional ion traps—both those made using hyperboloidal or curved electrodes (e.g., Paul trap, quadrupole mass filter and linear ion trap) and from traps made using planar metal electrodes (e.g., cylindrical trap, rectilinear trap). The electric field within the planar Paul trap is a function of the potentials applied to each ring, as well as the spatial arrangement of the rings and plates. As the RF potential on each ring is independently adjustable, there is a great deal of flexibility in constraining and optimizing the trapping field. As with any other ion trap, the shape of the electric field inside the trap plays an important role in determining the performance of the ion trap as a mass analyzer.

The ion motion for the present trap is governed by the RF electric field and by the auxiliary ac signal applied to the plates. Optimal electric fields for several trapping geometries have been reported by Ouyang el al.[12] In general, the performance of any ion trap is influenced by components of the electric field that are a higher order than quadrupolar (i.e., octopole). After investigation of the electric field for the cylindrical ion trap with different dimensions, Wu et al.[16] concluded that the increase of spectral resolution can be realized by appropriate compensation for high-order, nonlinear field components, particularly octopolar and dodecapolar fields. This approach was also used in the original Finnigan Ion Trap Detector, and was accomplished by increasing the spacing between electrodes.[17] Lammert and co-workers[11] reported that a certain amount of positive octopole contributed

to the increase of resolution of the toroidal ion trap.

For the planar Paul trap, the electric fields within the trapping volume were calculated, and voltages on individual rings optimized, using SIMION 7.[18] The nonlinear components of the axial electric field (along r=0) in the planar Paul trap were selected so as to be similar to those used in the asymmetric toroidal trap[11] and cylindrical ion trap.[16] During the course of optimization of electric fields, several sets of potentials were identified as feasible. The one chosen for this study, as given in Table 1, gave the greatest linear axial field of those examined. Surprisingly, the potentials on rings 1, 3, and 5 are all zero, resulting in an unusual feature in the electric field near the plate surfaces at these radii (observable in Figure 3(b)). It is not clear at this point why these values produced the best field among those examined, or whether there might be better sets of potentials possible. The permutation of possible values is large, and as yet no algorithm for complete optimization exists.

Figures 3(c) and (d) show the axial electric field ($E_z$) and non-linear contribution to the axial electric field ($\Delta E_z$) along the *z*-axis by subtracting a linear extrapolation of a narrow region of the derived electric field near the center of the trap, respectively. Similar to the electric fields in the traps mentioned above, the potential distribution used in the planar Paul trap included a small positive compensation of higher-order components, and is expected to improve the mass resolution of this novel trap. In contrast to methods used with other ion traps, however, the higher-order components were not added into the planar Paul trap by modifying the shape or arrangement of the electrodes, but rather by choosing the appropriate potential function that was applied to the set of rings. Changing the electric fields within the planar Paul trap is done by changing the values of the capacitors on the PCBs.

With the current plate spacing, only the first 11 rings had a noticeable effect on the electric fields in the trapping region. In order to save on cost, the plates were fabricated with additional rings, intended to be used in other experiments. In the present work, rings beyond ring 11 were shorted to ring 11.

In conventional three--dimensional ion traps, ion behavior is understood and predicted by reference to stability parameters in the Mathieu equation. The commonly-given form of the $q_z$ stability parameter from the Mathieu equation is:

$$q_z = \frac{8eV}{\left(r_0^2 + 2z_0^2\right)m\Omega^2} \quad (1)$$

where *m* and *e* are the mass and charge of an ion, $r_0$ and $z_0$ are the characteristic radial and axial dimensions of the trap, *V* is the zero-to-peak applied RF amplitude, and $\Omega$ is the RF frequency. This equation assumes purely quadrupolar potentials, but can be used for traps with small higher-order components. In the planar Paul trap, two parameters from Equation 1 are not obvious: there is no characteristic radial dimension, and the applied voltage is ambiguous. The $q_z$ parameter can nevertheless be estimated by examining the potential at any radius using SIMION. For convenience, the voltage is calculated at a radius that would correspond with the ring electrode in a conventional ion trap, in other words, at

$$r = \sqrt{2}z_0 . \quad (2)$$

Using this approach, and the potentials given in Table 1, the high-mass limit of

the planar Paul trap (at $q_z$ = 0.908) should be 195 m/z. For resonant ejection at $\beta$ = 0.46, the high-mass limit of the trap should be 275. The low-mass limit depends on the lowest RF amplitude applied to the trap, and can be similarly calculated.

## RESULTS AND DISCUSSION

**Ejection method.** The performance of the planar Paul trap mass analyzer was tested using three modes of ion ejection: boundary ejection, quadrupole resonant ejection, and dipole resonant ejection. Boundary ejection, in which the RF amplitude is ramped and ions eject spontaneously at $q_z$ = 0.908, was used historically in Paul traps, but is not currently in common use.[19] Quadrupole[20] and dipole[21,22] resonant ejection rely on applying a small supplementary ac signal to the trap. Ions are ejected when the supplementary signal resonantly excites the secular motion of ions. Ions can be ejected either just before the $q_z$ = 0.908 boundary, or at significantly lower $q_z$ values.

During the development of planar Paul ion trap, changes in the ion ejection mode were found to affect mass resolution. Figure 4 shows three arrangements (boundary ejection, quadrupole ejection and dipole ejection) for the applications of an auxiliary ac potential to the planar Paul trap. Supplemental ac signals were connected to the innermost ring in each case. Comparisons of spectra obtained with these three arrangements were made using toluene as the sample, as illustrated in Figure 4. When boundary ejection was performed without application of a supplementary ac voltage to the trapping plates, the mass resolution was far too low to resolve peaks *m/z* 91 and 92, and peak intensity was poor (Figure 4(a)). After the supplementary ac voltage was applied to the trapping plates, the resolution for spectra of toluene was greatly improved. As the in-phase potentials were applied to both of trapping plates (quadrupole ejection), the resolution ($m/\Delta m$, FWHM definition) for peak *m/z* 91 from toluene was about 370 (Figure 4(b)). The resolution was increased to ca. 700, as given in Figure 4(c), when out-of-phase potentials were applied to both trapping plates (dipole ejection), which is due to the kinetic excitation of ions when the frequency of the supplementary ac voltage coincides with one of their secular oscillation frequencies.[23] Therefore, dipole ejection was used for subsequent experiments.

**Scan rate**. It is well known[24-27] that decreasing the RF scan rate can improve mass resolution in ion traps. Figure 5 shows mass spectra of the molecular ion region of toluene and demonstrates the improvement in resolution obtained by varying the RF scan rate. The peaks of *m/z* 91 and 92 were partially resolved at a scan rate of 7074 Th/s, as shown in Figure 5(a). With the decrease of scan rate to 3583 Th/s, the peaks are almost resolved from each other (Figure 5(b)). The mass spectrum that shows baseline separation of peaks 91 and 92 was recorded by further decreasing the scan rate to 1792 Th/s and 862 Th/s, and mass resolution at FWHM of 0.26 and 0.12 for *m/z* 91, as shown in Figure 5(c) and 5(d), was obtained. From the above results, the resolution is enhanced ca. 4.5-fold by reduction of the mass scan rate by a factor of about 8.2, which can be attributed to the increased number of increments of the rf voltage in a given mass range and the increased time

allowed for ions with adjacent *m/z* values to be ejected at the threshold of their instability.[24, 28-31] Mass accuracy was compared between the different RF scan rates, and is given in Table 2. With the increase of scan rate from 862 Th/s to 7074 Th/s, the mass shift increases with an exception at a scan rate of 7074 Th/s for peak *m/z* 91. The mass shift in this case could be due to ripple or inconsistencies in the power supplies or frequencies used to operate the trap, or could result from space-charge effects.

**Dynamic range.** Experiments were carried out over a range of sample pressures from $10^{-5}$ torr to $10^{-3}$ torr. The number of ions detected at each pressure was adequate for quantitation. Dynamic range is an issue in all ion trap devices, because ion density in the trapping region must be small enough that the perturbation to the electric field is minimal. In Paul-type traps methods such as Automatic Gain Control (AGC) are used to improve experimental dynamic range. Linear, rectilinear, and toroidal ion traps have a larger storage volume, and therefore an inherently higher dynamic range. Trap arrays can also be used to improve performance in this regard. The planar Paul trap is expected to have a dynamic range limited by the small trapping volume (typical of other Paul-type traps) and by the low operating voltage used.

## CONCLUSION

A novel mass analyzer, the planar Paul ion trap with resistive electrodes, has been designed and constructed. SIMION 7 was used to determine the potential function on a planar resistive material such that the electric field within the trapping region would be primarily quadrupolar, with a small positive octopole contribution. Both dipolar and quadrupolar resonant ejection improved mass resolution over a simple boundary scan. Mass resolution is enhanced by reduction of the scan rate. The data reported here show that the electric field produced by the trapping plates, rather than the conventional shaped electrodes, is applicable to perform mass spectra of various compounds, and high resolution can be obtained. While mass resolution observed in these experiments is reasonably high, the present system is not optimized in several ways. Limitations to resolution may be due to electronic jitter or noise, due to electric field shape, space-charge, or other effects.

The present study also demonstrates the use of microfabricated plates to create and modify quadrupolar trapping fields. Desirable electric fields can be created without the issues that arise from machining precision or complex electrode shapes. That this approach has also been used to produce a toroidal trapping geometry[13] illustrates the versatility of such plates in producing various electric field configurations. Future work on the planar Paul trap is aimed at improving mass resolution, performing tandem MS experiments, and better understanding the electric fields within the trap.

## REFERENCES


(1) Paul, W.; Steinwedel, H. *Z. Naturforsch.* **1953**, *8A*, 448-450.

(2) Wells, J. M.; Badman, E. R.; Cooks, R. G. *Anal. Chem.* **1998**, *70*, 438-444.

(3) Dawson, P. H.; Hedman, J.; Whetten, N. R. *Rev. Sci. Instrum.* **1969**, *40*, 1444-1450.

(4) Lawson, G.; Bonner, R. F.; Todd, J.

F. J. *J. Phys. E* **1973**, *6*, 357-362.
(5) Badman, E. R.; Johnson, R. C.; Plass, W. R.; Cooks, R. G. *Anal. Chem.* **1998**, *70*, 4896-4901.
(6) Dobson, G. S.; Enke, C. G. *Anal. Chem.* **2007**, *79*, 3779-3785.
(7) Tabert, A. M.; Griep-Raming, J.; Guymon, A. J.; Cooks, R. G. *Anal. Chem.* **2003**, *75*, 5656-5664.
(8) Patterson, G. E.; Guymon, A. J.; Riter, L. S.; Everly, M.; Griep-Raming, J.; Laughlin, B. C.; Ouyang, Z.; Cooks, R. G. *Anal. Chem.* **2002**, *74*, 6145-6153.
(9) Erickson, B. E. *Anal. Chem.* **2004**, *76*, 305A.
(10) Janfelt, C.; Graesboll, R.; Lauritsen, F. R. *Int. J. Mass Spectrom*. **2008**, *276*, 17-23.
(11) Lammert, S. A.; Plass, W. R.; Thompson, C. V.; Wise, M. B. *Int. J. Mass Spectrom.* **2001**, *212*, 25–40.
(12) Ouyang, Z.; Wu, G.; Song, Y.; Li, H.; Plass, W. R.; Cooks, R. G. *Anal. Chem.* **2004**, *76*, 4595-4605.
(13) Austin, D. E.; Wang, M.; Tolley, S. E.; Maas, J. D.; Hawkins, A. R.; Rockwood, A. L.; Tolley, H. D.; Lee, E. D.; Lee, M. L. *Anal. Chem.* **2007**, *79*, 2927–2932.
(14) Xu, W.; Chappell, W. J.; Cooks, R. G.; Ouyang, Z. *J. Mass Spectrom.* **2008**, DOI: 10.1002/jms.1512.
(15) Austin, D. E.; Peng, Y.; Hansen, B. J.; Miller, I. W.; Rockwood, A. L.; Hawkins, A. R.; Tolley S. E. *J. Am. Soc. Mass Spectrom.* **2008**, *19*, 1435-1441.
(16) Wu, G.; Cooks, R. G.; Ouyang, Z. *Int. J. Mass Spectrom.* **2005**, *241*, 119–132.
(17) Franzen, J.; Gabling, R.-H.; Schubert, M.; Wang, Y. In *Practical Aspects of Ion Trap Mass Spectrometry*; March, R. E., Todd, J. F. J., Eds.; CRC Press: New York, USA, 1995; Vol. 1, pp 66-69.
(18) Dahl, D. A. *SIMION Version 7.0*. Idaho national engineering and environmental laboratory: Idaho Falls, ID, **2000**.
(19) Traldi, P.; Catinella, S.; March, R. E.; Creaser, C. S. In *Practical Aspects of Ion Trap Mass Spectrometry*; March, R. E., Todd, J. F. J., Eds.; CRC Press: New York, USA, 1995; Vol. 1, pp 229-341.
(20) March, R. E.; McMahon, A. W.; Londry, F. A.; Alfred, R. L.; Todd, J. F. J.; Vedel, F. *Int. J. Mass Spectrom. Ion Process*. **1989**, *95*, 119-156.
(21) Ioanoviciu, D.; Ioanoviciu, A. S. *Nucl. Instrum. Methods Phys. Res. A.* **1999**, *427*, 161-165.
(22) Zhao, X. Z.; Douglas, D. J. *Int. J. Mass Spectrom*. **2008**, *275*, 91-103.
(23) Goeringer, D. E.; Whitten, W. B.; Ramsey, J. M.; McLuckey, S. A.; Glish G. L. *Anal. Chem*. **1992**, *64*, 1434-1439.
(24) Schwartz, J. C.; Syka, J. E. P.; Jardine, I. *J. Am. Soc. Mass Spectrom*. **1991**, *2*, 198-204.
(25) Goeringer, D. E.; McLuckey, S. A.; Glish, G. L. *Proceedings of the 39th Annual Conference of Mass Spectrometry and Allied Topics*, Nashville, TN, **1991,** p532.
(26) Williams, J. D.; Cox, K.; Morand, K. L.; Cooks, R. G.; Julian, R. K., Jr.; Kaiser, R. E. *Proceedings of the 39th Annual Conference of Mass Spectrometry and Allied Topics*, Nashville, TN, **1991,** p1481.
(27) Kaiser, R. E.; Cooks, R. G.; Stafford, G. C.; Syka, J. E. P.; Hemberger, P. H. *Int. J. Mass Spectrom. Ion Processes* **1991**, *106*, 79-115.
(28) Williams, J. D.; Cox, K. A.; Cooks, R. G.; Kaiser, R. E.; Schwartz, J. C. *Rapid Commun. Mass Spectrom.* **1991**, *5*, 327-329.

(29) Makarov, A. A. *Anal. Chem.* **1996**, *68*, 4257-4263.
(30) Schwartz, J. C.; Senko, M. W.; Syka, J. E. P. *J. Am. Soc. Mass Spectrom.* **2002**, *13*, 659-669.
(31) Song, Q.; Kothari, S.; Senko, M. A.; Schwartz, J. C.; Amy, J. W.; Stafford, G. C.; Cooks, R. G.; Ouyang, Z. *Anal. Chem.* **2006**, *78*, 718-725.

**Figure Captions**

**Figure 1.** (a) Top-view diagram of electrode plate and (b) the instrument setup for the experiments.

**Figure 2.** Timing diagram for the planar Paul ion trap. The four stages are dump, ionization, cool, and analysis/ejection scan. In the dump stage, the RF is turned off to eject trapped ions that were not ejected during the previous analysis/ejection scan. The ionization stage turns on the trapping RF and turns the filament bias voltage to -50 V (electron gun on). The cool stage turns the filament bias voltage back to +180 V (electron gun off), while maintaining the trapping RF in order to cool the ions. The final stage, analysis/ejection scan, keeps the trapping RF on, and turns the ejection AC on in combination of sweeping the voltage of the ejection AC.

**Figure 3.** Schematics of (a) the trapping plates, (b) electric field distribution, (c) axial electric field ($E_z$) and (d) non-linear high-order distribution to the axial electric field ($\Delta E_z$) along the *z*-axis in the planar Paul trap.

**Figure 4.** Mass spectra of toluene recorded at different ejection modes: (a) the centers of both trapping plates grounded (boundary ejection); (b) in-phase potentials applied to both trapping plates (quadrupole ejection); and (c) out-of-phase potentials applied to both trapping plates (dipole ejection) with applied supplementary ac signal of 290 kHz, 3.5 $V_{0\text{-}p}$, $P_{toluene}$ = 1.0 x $10^{-5}$ Torr, $P_{helium}$ = 5.34 x $10^{-3}$ Torr, ionization time = 4 ms.

**Figure 5.** Mass spectra of toluene showing the doublet *m/z* 91 and 92, recorded at different RF scan rates using dipole ejection mode with applied supplementary ac voltage of 290 kHz, 3.5 $V_{0\text{-}p}$. $P_{toluene}$ = 1.0 x $10^{-5}$ Torr, $P_{helium}$ = 5.34 x $10^{-3}$ Torr, ionization time = 4 ms.

**Table 1.** Dimensions and optimized RF amplitudes applied to each ring.

**Table 2.** Observed mass shifts for peaks *m/z* 91 and 92 using various RF scan rates.

# Figure 1

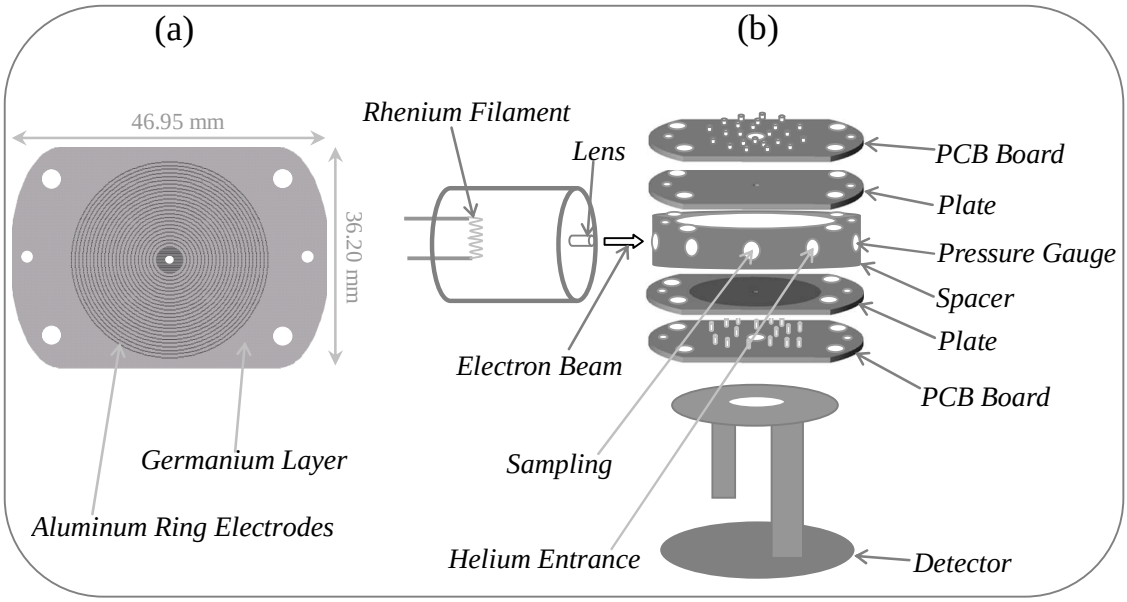


# Figure 2

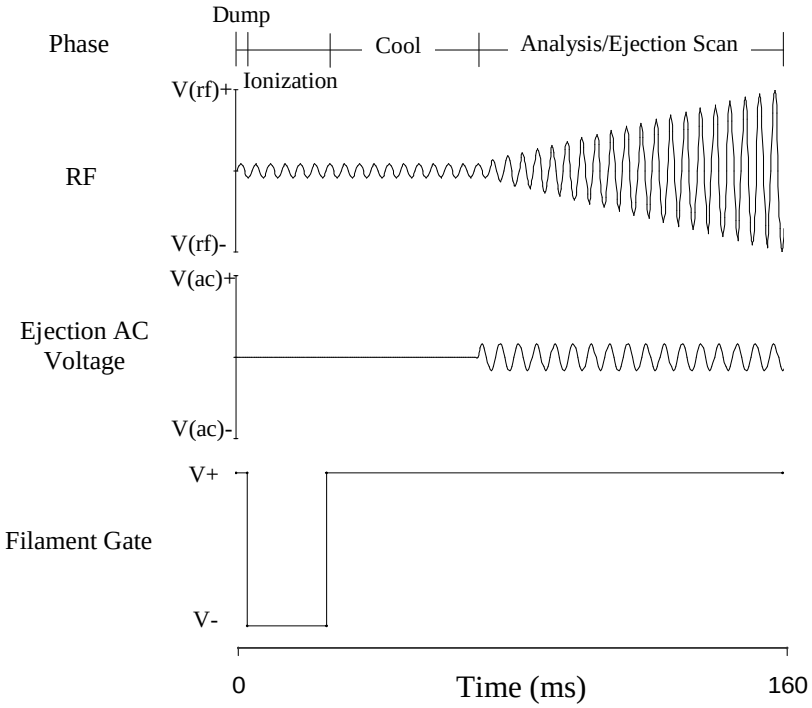

# Figure 3

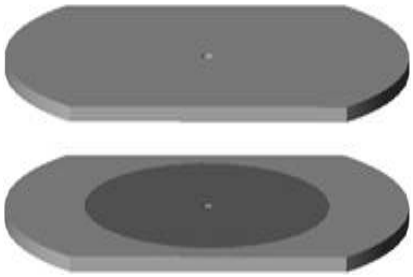

(a)

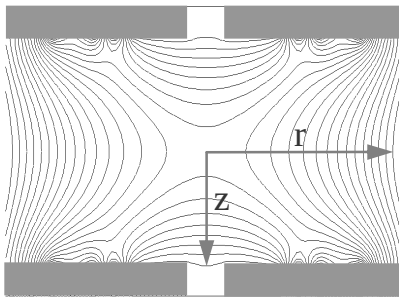
r
z

(b)

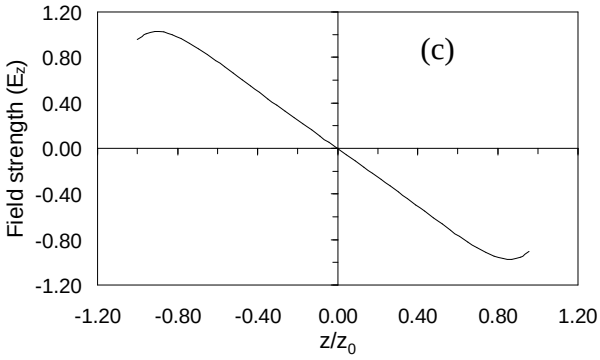
(c)
Field strength (Ez)
1.20
0.80
0.40
0.00
-0.40
-0.80
-1.20
-1.20
-0.80
-0.40
0.00
0.40
0.80
1.20
z/z0

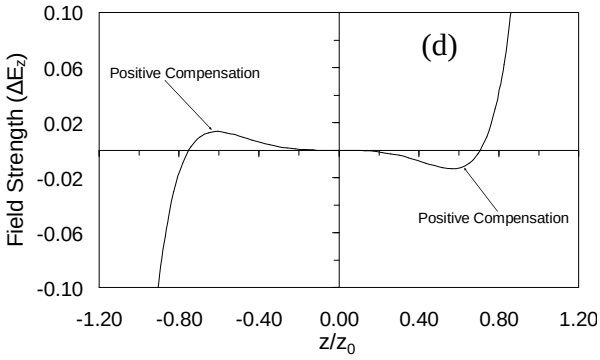
(d)
Field Strength (ΔEz)
0.10
0.06
0.02
-0.02
-0.06
-0.10
Positive Compensation
Positive Compensation
-1.20
-0.80
-0.40
0.00
0.40
0.80
1.20
z/z0

# Figure 4

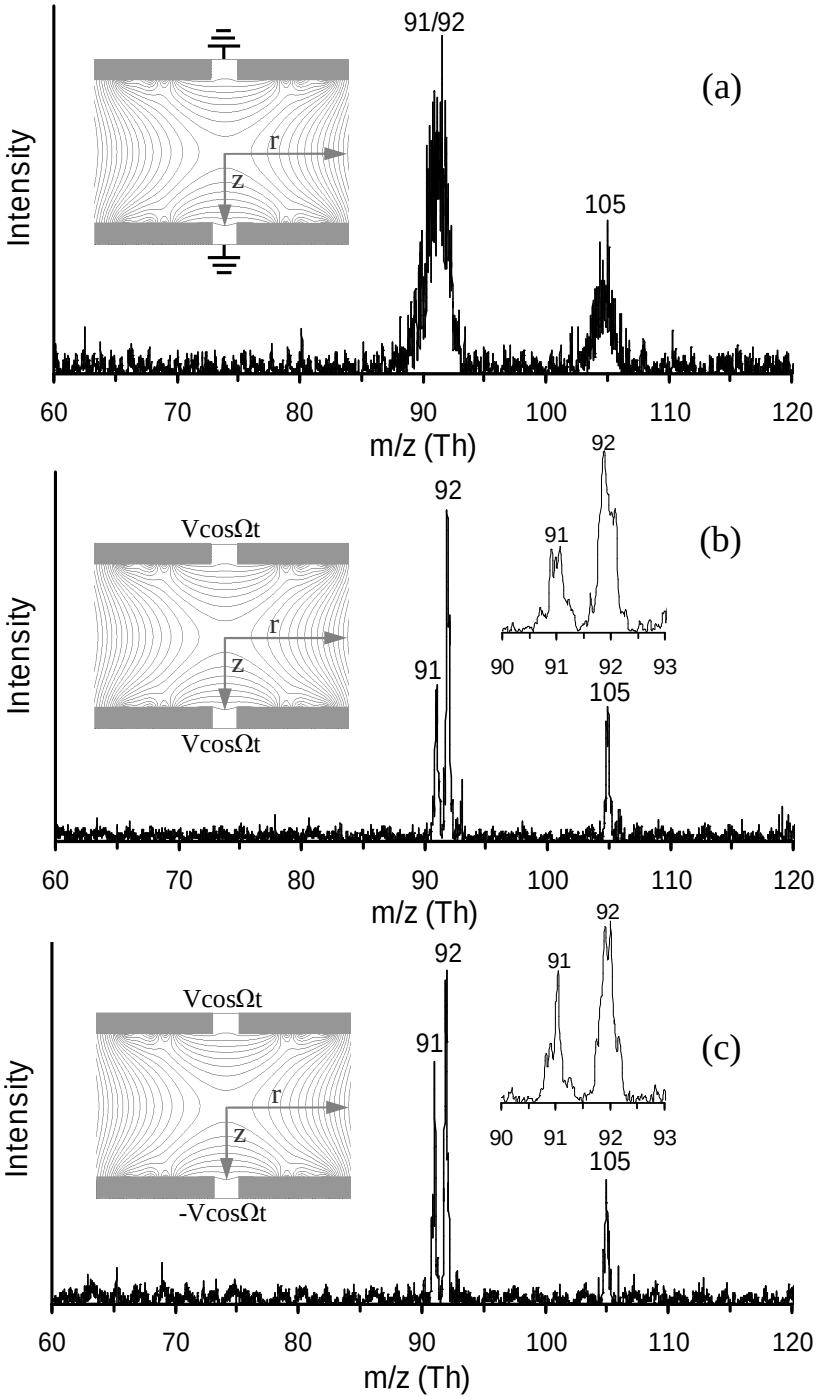
91/92
(a)
Intensity
r
z
105
60
70
80
90
100
110
120
m/z (Th)
92
91
(b)
VcosΩt
VcosΩt
90
91
92
93
105
(c)
-VcosΩt

# Figure 5

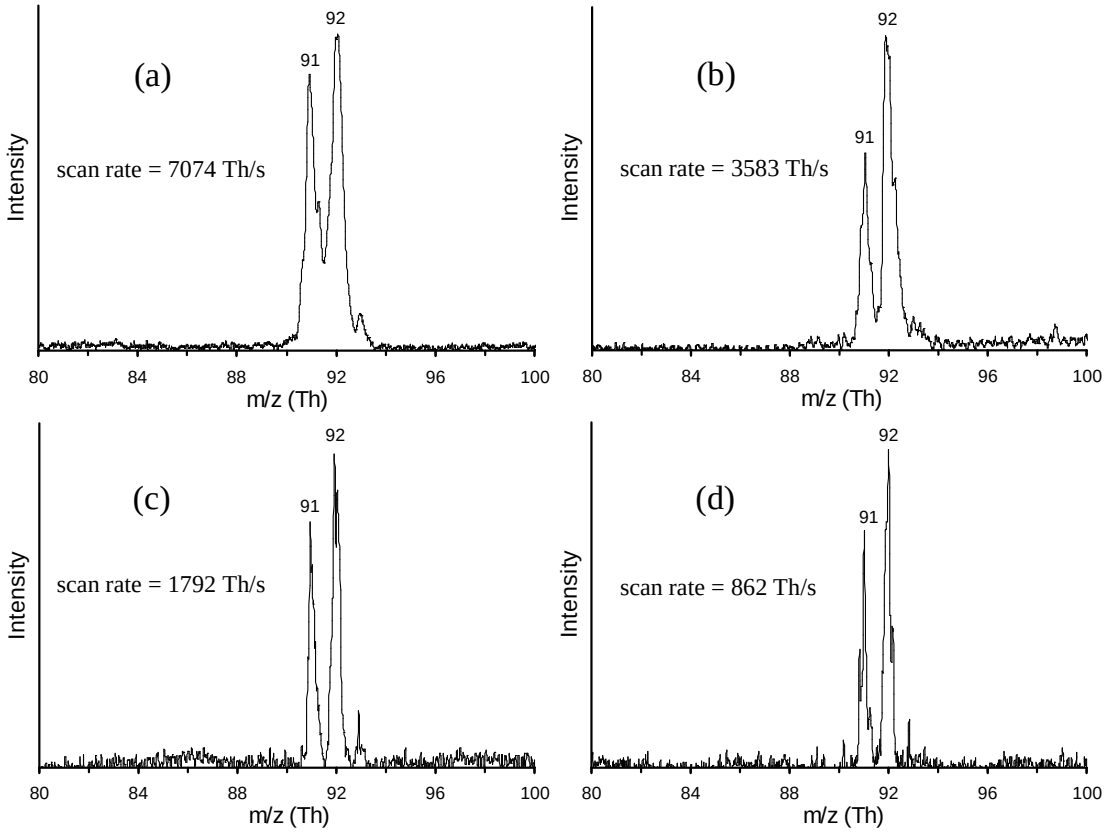
(a)
scan rate = 7074 Th/s
91
92
Intensity
80
84
88
92
96
100
m/z (Th)
(b)
scan rate = 3583 Th/s
91
92
Intensity
80
84
88
92
96
100
m/z (Th)
(c)
scan rate = 1792 Th/s
91
92
Intensity
80
84
88
92
96
100
m/z (Th)
(d)
scan rate = 862 Th/s
91
92
Intensity
80
84
88
92
96
100
m/z (Th)

# Table 1

**Table 1. Dimensions and Optimized RF Amplitudes Applied to Each Ring**

| Ring No. | Inner radius (mm) | Outer radius (mm) | RF amplitude ($V_{0\text{-}p}$) |
|---|---|---|---|
| 1 | 0.5 | 1.8 | 0 |
| 2 | 2.2 | 2.3 | 241 |
| 3 | 2.7 | 2.8 | 0 |
| 4 | 3.2 | 3.3 | 90 |
| 5 | 3.7 | 3.8 | 0 |
| 6 | 4.2 | 4.3 | 241 |
| 7 | 4.7 | 4.8 | 350 |
| 8 | 5.2 | 5.3 | 400 |
| 9 | 5.7 | 5.8 | 480 |
| 10 | 6.2 | 6.3 | 680 |
| 11-24 | 6.7-13.2 | 6.8-13.3 | 738 |

# Table 2

**Table 2. Observed Mass Shifts for Peaks *m/z* 91 and 92 using various RF Scan Rates**

| Scan rate (Th/s) | $\Delta\,(m/z)_{91}$ | $\Delta\,(m/z)_{92}$ |
|---|---|---|
| 862 | 0.028 | 0.011 |
| 1792 | -0.046 | 0.035 |
| 3583 | 0.060 | -0.044 |
| 7074 | -0.053 | 0.081 |